Proofs to: Dr. George Britovsek
Department of Chemistry
Imperial College London
Exhibition Road
South Kensington
London SW7 2AY
UK
Tel. +44-(0)20-75945863
Fax. +44-(0)20-75945804
e-mail: g.britovsek@imperial.ac.uk

Catalyst Stability Determines the Catalytic Activity of Non-Heme Iron Catalysts in the Oxidation of Alkanes

Jason England, Catherine R. Davies, Maria Banaru, Andrew J.P. White and George J.P. Britovsek,*

Department of Chemistry, Imperial College London, Exhibition Road, London, SW7 2AY, UK.

Abstract

A series of iron(II) bis(triflate) complexes [Fe(L)$(OTf)_2$] containing linear tetradentate bis(pyridylmethyl) diamine ligands with a range of ligand backbones has been prepared. The backbone of the ligand series has been varied from a two-carbon linkage (ethylene (**1**), 4,5-dichlorophenylene (**2**) and cyclohexyl (**3**)) to a three-carbon (propyl (**4**)) and a four-carbon linkage (butyl (**5**)). The coordination geometries of these complexes have been investigated in the solid state by X-ray crystallography and in solution by ^{1}H and ^{19}F NMR spectroscopy. Due to the labile nature of high spin iron(II) complexes in solution, dynamic equilibria of complexes with different coordination geometries (*cis*-α, *cis*-β and *trans*) are observed with ligands **2**–**5**. In these cases, the geometry observed in the solid state does not necessarily represent the only or even the major geometry present in solution. The ligand field strength in the various complexes has been investigated by VT magnetic moment measurements and UV-vis spectroscopy. The strongest ligand field is observed with the most rigid ligands **1** and **2**, which generate complexes [Fe(L)$(OTf)_2$] with a *cis*-α coordination geometry and the corresponding complexes $[Fe(L)(CH_3CN)_2]^{2+}$ displays spin crossover behaviour. The catalytic properties of the complexes for the oxidation of cyclohexane, using hydrogen peroxide as the oxidant, have been investigated. An increased flexibility in the ligand results in a weaker ligand field, which increases the lability of the complexes. The activity and selectivity of the catalysts appear to be related to the strength of the ligand field and the stability of the catalyst in the oxidising environment.

Introduction

The ability to selectively oxidise unfunctionalised alkanes has been a long-standing goal and challenge in catalysis research.[1-4] A number of different classes of oxidation catalysts have been developed during the last 50 years, for example heme-based iron complexes containing porphyrin-type ligands,[5] polyoxometalates[6-8] and recently also organic non-metal catalysts.[9-11] The catalysts are typically combined with oxidants, which can have different oxo transfer abilities[12], for example H_2O_2, O_2, ClO^-, PhIO, O_3 or N_2O, whereby the first two oxidants are economically and environmentally the most attractive oxidants.[13, 14] A relatively recent addition to the armoury of oxidation catalysts has been a class of non-heme iron catalysts, inspired by nature's use of non-heme iron-based enzymes for the selective oxidation of C-H bonds.[15-19]

An attractive feature of non-heme iron catalysts is that ligand modifications and catalyst tuning are relatively straightforward, compared for example with heme-type ligand systems. However, many of the non-heme iron complexes that have been used as catalysts in combination with H_2O_2 have shown catalytic behaviour that resembles simple Fenton-type chemistry,[20] which is characterised by low conversions, low product selectivities and extensive H_2O_2 decomposition. In contrast, much higher conversions of H_2O_2 into oxidised product combined with a more selective oxidation reactivity have been observed with non-heme iron(II) catalyst containing either tripodal tetradentate ligands such as TPA[21, 22] or *iso*-BPMEN (see Figure 1),[23] or linear tetradentate ligands such as BPMEN[24] or BQEN.[25] In addition, these catalysts have shown stereospecific and dioxygen-independent hydroxylation of alkanes.[16, 26, 27] and the C-H regio-selectivities and kinetic isotope effects are also indicative of a more selective oxidant than those responsible for oxidation in Fenton-type systems. Isotope labelling studies[28] and DFT calculations[29] implicate a high valent iron oxo complex as the active oxidant,[30, 31] which suggests that the reaction mechanism could be analogous to the mechanism for Cytochrome P-450 systems,[5] (hydrogen atom abstraction followed by a rapid oxygen rebound).[32]

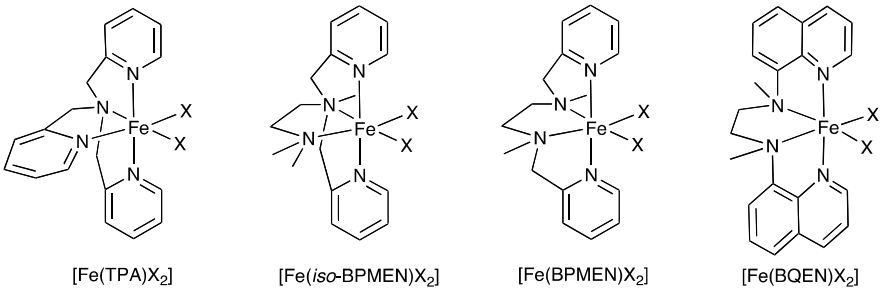

Figure 1. Examples of non-heme iron(II) oxidation catalysts.

Common features in these non-heme iron catalysts are the use of tetradentate ligands with at least two pyridine-type donors and two *cis* labile co-ligands X, for example weakly coordinating triflate anions or acetonitrile molecules in combination with non-coordinating anions. Iron(II) complexes containing linear tetradentate ligands such as BPMEN or BQEN are currently the most efficient catalysts for the oxidation of alkanes using H_2O_2 as the oxidant. One of the main questions that immediately arises is: Why are these particular catalysts so much better than other non-heme iron(II) catalysts? In our attempt to address this question, we have been systematically investigating the ligand-based requirements that are needed for the formation of efficient catalysts for the oxidation of alkanes using H_2O_2 as the oxidant. Here we report our results regarding a series of iron(II) complexes with ligands **1** – **5** incorporating pyridylmethyl units and a range of different ligand backbones (see Figure 2). The length of the backbone has been varied from 2 to 4 carbon atoms resulting in various degrees of ligand flexibility. The coordination geometries of the iron(II) bis(triflate) complexes have been determined in the solid state and in solution. The spectroscopic and magnetic properties of the iron(II) complexes have been measured, in an attempt to correlate the coordination geometry with the catalytic activity and selectivity of these complexes for the oxidation of cyclohexane. Ligands **1**, **3** and **4** and their iron(II) complexes have been used previously as catalysts for the oxidation of alkanes or alkenes.[23, 33-37] Here we will report on some novel aspects of their solution behaviour and their spectroscopic and magnetic properties. In addition, their inclusion in this series has allowed us to establish trends on the geometrical behaviour of iron(II) complexes containing linear tetradentate ligands and the relationship with their catalytic activity. Ligand rigidity and a strong ligand field appear to be critically important for high catalytic activity, which is related to catalyst stability and lifetime under the harsh oxidising conditions.

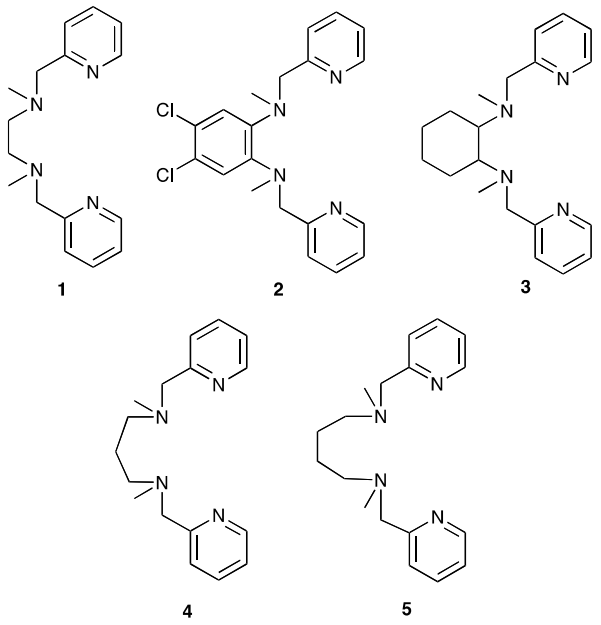

Figure 2. Backbone variations in bis(pyridylmethyl)diamine ligands **1** – **5**.

Results and Discussion

Synthesis of ligands and complexes

The synthesis and characterisation of the ligands **1**, **3** and **4** and their corresponding iron(II) bistriflate complexes have been reported previously.[23, 33, 34, 37, 38] Ligand **5** was prepared by the condensation of pyridine carboxaldehyde with 1,4-butanediamine, followed by reduction with $NaBH_4$. This leads initially to the known N,N'-bis(2-pyridylmethyl)butyl diamine,[39] which was methylated to give ligand **5** in good yield. This procedure does not work for ligand **2**. The preparation of the corresponding non-methylated secondary amine 1,2-bis(2-pyridylmethylamino)benzene has previously been reported by Miyano and co-workers by the reaction of benzene-1,2-diamine with pyridine-2-carbinol at elevated temperatures in the presence of catalytic amounts of pyridine N-oxide.[40] However, we were unable to reproduce these results and only starting materials were obtained using this method. The attempted preparation of 1,2-bis(2-pyridylmethylamino)benzene by reductive amination of 1,2-diaminobenzene using pyridine-2-carboxaldehyde and sodium triacetoxyborohydride was complicated by the formation of an aminal side-product (Equation 1). Attempts to separate the aminal product from the desired amine product were unsuccessful, as were attempts to eliminate its formation by modification of the reaction conditions. Furthermore,

the aminal was found to emerge unscathed from attempted hydrolysis and reduction, even under particularly harsh conditions (e.g. reduction using $LiAlH_4$). Attempts to circumvent this problem by using a one-step preparation of the targeted ligand by reductive amination of N,N'-dimethyl-1,2-diaminobenzene using pyridine-2-carboxaldehyde and sodium triacetoxyborohydride as the reductant yielded only the corresponding aminal product.

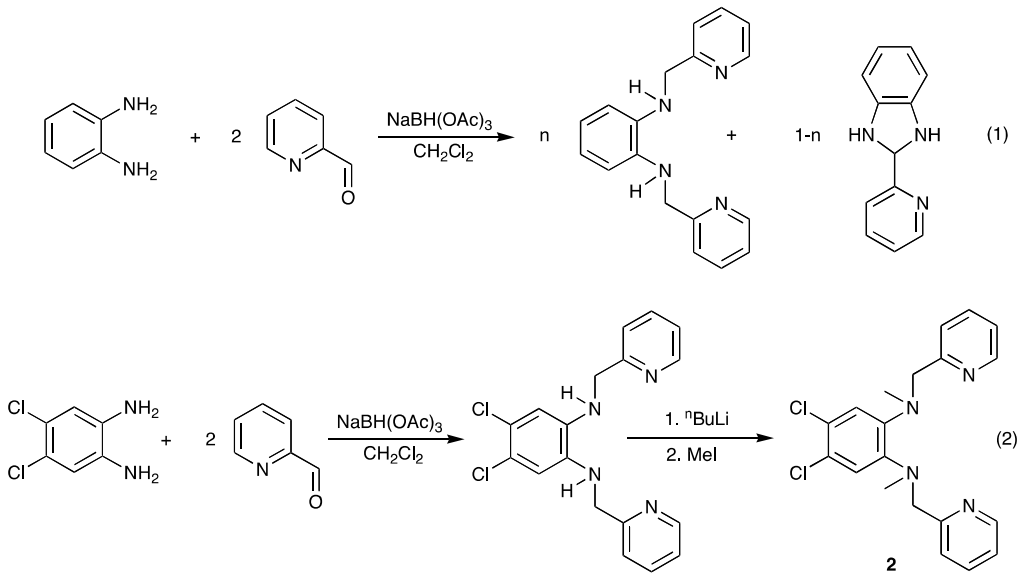

It was found that the use of the less nucleophilic 4,5-dichloro-1,2-diaminobenzene in place of 1,2-diaminobenzene in the reductive amination procedure, using excess pyridine-2-carboxaldehyde and sodium triacetoxyborohydride, suppressed aminal formation. Unlike the non-chlorinated analogue, the diamine product was found to be a solid. This allowed straightforward purification by recrystallisation from ethanol. Deprotonation with 2 equivalents of n-butyl lithium yielded the corresponding lithium diamide, which after subsequent reaction with methyl iodide gave the desired ligand **2** in near quantitative yield (Equation 2).

The iron(II) complexes [Fe(**1**)$(OTf)_2$], [Fe(**2**)$(OTf)_2$], [Fe(**3**)$(OTf)_2$], [Fe(**4**)$(OTf)_2$] and [Fe(**5**)$(OTf)_2$] were prepared by mixing tetrahydrofuran (THF) solutions of equimolar quantities of ligands and $Fe(OTf)_2(CH_3CN)_2$ at room temperature. The complexes precipitate from THF and are easily purified by recrystallisation. Interestingly, the formation of the C_2-bridged complexes [Fe(**1**)$(OTf)_2$], [Fe(**2**)$(OTf)_2$] and [Fe(**3**)$(OTf)_2$] typically requires less than a day before product precipitation occurs from THF, whereas several days are required for [Fe(**4**)$(OTf)_2$] and several weeks for complex [Fe(**5**)$(OTf)_2$], which indicates quite

different rates of complex formation. The solid state structures of complexes [Fe(**2**)$(OTf)_2$] and [Fe(**4**)$(OTf)_2$] have been determined by X-ray analysis and the coordination behaviour in solution has been investigated for all complexes by ^{1}H and ^{19}F NMR, UV-Vis spectroscopy and magnetic susceptibility measurements.

Solid State Structures

Solid state X-ray analysis of crystals of [Fe(**2**)$(OTf)_2$] revealed a *cis*-α coordination mode (see Figure 3). Whereas the plane defined by the iron centre and the two triflate oxygens {Fe,O(31),O(41)}and the plane defined by the iron centre and the two pyridine nitrogens {Fe,N(1),N(22)} are nearly orthogonal (88.4˚), the angle ϕ between the {Fe,O(31),O(41)} plane and the {Fe,N(8),N(15)} plane is 17˚ (see Figure 4). The analogous angle ϕ in the complex [Fe(**1**)Cl_2] is 14˚ (the angle between the other two planes is 87.4˚),[41] which indicates a less favourable orbital overlap between the amine donors and the iron centre in the case of complex [Fe(**2**)$(OTf)_2$] due to the rigid phenylene backbone. The configurations of the amine nitrogen atoms are the same ((*R*,*R*) in the stereoisomer shown in Figure 3). The Fe–bond distances are typical for high spin iron(II) complexes, with those to the *trans* pyridyl nitrogens being *ca.* 0.1 Å shorter than those to the amino nitrogens N(8) and N(15). A similar pattern is seen in the related complex [Fe(**1**)$(Cl)_2$], though it is notable that in this C_2-symmetric *cis*-α complex, the Fe–N(pyridyl) and Fe–N(amino) distances [2.195(4) and 2.278(4) Å respectively] are both longer than seen here in [Fe(**2**)$(OTf)_2$].[41]

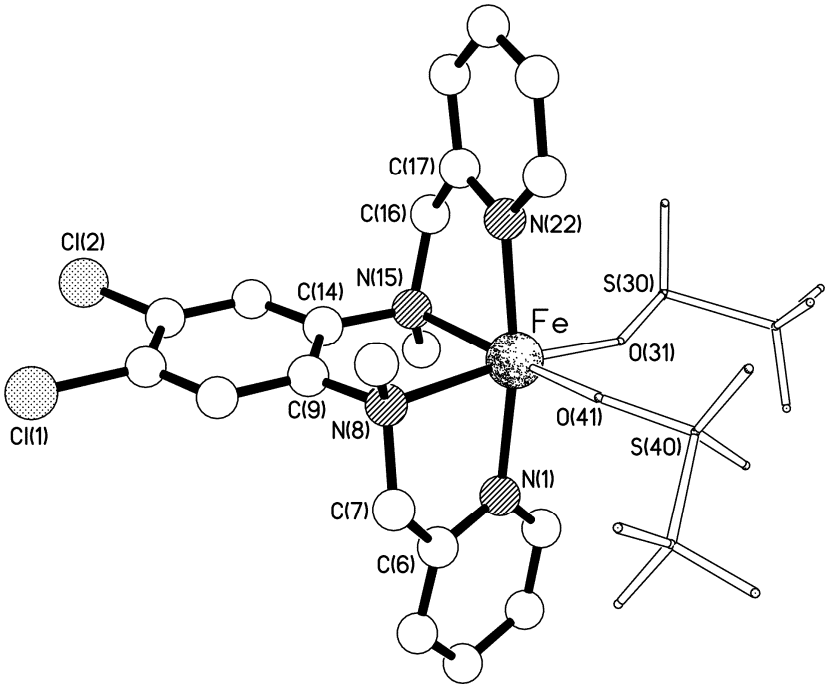

Figure 3. The molecular structure of [Fe(**2**)$(OTf)_2$].

Table 1. Selected bond lengths (Å) and angles (°) for the two independent complexes (**I** and **II**) present in the crystals of [Fe(**2**)$(OTf)_2$].

	Mol I	**Mol II**			**Mol I**	**Mol II**
Fe–N(1)	2.154(2)	2.154(2)		Fe–N(8)	2.2340(19)	2.227(2)
Fe–N(15)	2.236(2)	2.233(2)		Fe–N(22)	2.138(2)	2.154(2)
Fe–O(31)	2.069(2)	2.0958(19)		Fe–O(41)	2.1037(18)	2.0798(19)
N(1)–Fe–N(15)	93.63(8)	94.69(8)		N(1)–Fe–N(8)	78.83(7)	78.68(8)
N(1)–Fe–N(22)	170.21(8)	171.12(8)		N(1)–Fe–O(31)	90.76(9)	91.06(8)
N(1)–Fe–O(41)	94.33(8)	93.60(8)		N(8)–Fe–N(15)	80.49(7)	80.68(7)
N(8)–Fe–N(22)	94.36(8)	94.77(8)		N(8)–Fe–O(31)	168.95(9)	167.13(7)
N(8)–Fe–O(41)	89.37(7)	90.07(8)		N(15)–Fe–N(22)	78.20(8)	78.21(8)
N(15)–Fe–O(31)	96.62(8)	92.58(8)		N(15)–Fe–O(41)	165.65(8)	166.12(8)
N(22)–Fe–O(31)	95.49(9)	94.55(8)		N(22)–Fe–O(41)	92.60(8)	92.38(8)
O(31)–Fe–O(41)	95.19(9)	98.38(8)				

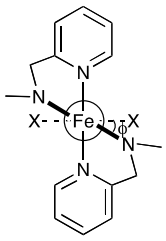

Figure 4. Definition of the angle ϕ.

During this work the single crystal X-ray structure of the dichloromethane solvate of [Fe(**4**)(OTf)$_2$] was determined. The structure is essentially the same as that of the non-solvated complex reported recently by Que and coworkers,[37] and shows that the propyl-bridged ligand adopts the *trans* coordination geometry, whereby the amine N centres have the opposite configurations (*R,S* or *S,R*). Given that in addition to this earlier report, the tetradentate ligand in our determination is highly disordered, we have reported our structure in the supporting information.

Geometrical Isomerisations and Ligand Dynamics

Linear tetradentate ligands can adopt three coordination modes in octahedral metal complexes: *cis*-α, *cis*-β and *trans*. The two internal donors become chiral upon coordination to the metal and can therefore have either the same or opposite configuration. Assuming that the configuration of these internal two donors remains unchanged, this increases the number of possible isomers to five pairs of enantiomers: *cis*-α (*R,R* or *S,S*), *cis*-β (*R,R* or *S,S*) or *cis*-β (*R,S* or *S,R*) and *trans* (*R,R* or *S,S*) or *trans* (*R,S* or *S,R*). From molecular models it is immediately evident that the *cis*-α (*R,S* or *S,R*) geometry is not possible due to severe bite-angle strain within the complex. Whichever geometry a linear tetradentate ligand will adopt preferentially in a metal complex is not easily predicted and depends on a number of factors, including the number of atoms between the donors, the solvent and the temperature. In addition, if the co-ligands are labile such as triflate or acetonitrile ligands, equilibria can exist between the different geometries in solution, which will be concentration and temperature dependent. The coordination geometries observed in the solid state are therefore not necessarily the same as those in solution, as we have previously established for a series of iron(II) complexes containing bis(quinolyl)diamine ligands.[25]

Bosnich and co-workers have analysed the relative stability of a series of Co(III) complexes containing the linear tetradentate tetraamine ligands, 2,2,2-tet, 3,2,3-tet and 2,3,2-tet, whereby the numbers denote the number of bridging atoms between the four amine donors.[42] The preference for any of the three possibly topologies, *cis*-α, *cis*-β or *trans*, depends on the cumulative bite-angle strain of the three chelate rings formed by the linear tetradentate ligand, which in turn is related to the absolute configuration of the chirality at the internal amine donors. Unlike the kinetically inert low-spin Co(III) complexes, for which different conformational isomers can often be isolated, the labile high-spin iron(II)

complexes here show rapid equilibria between different isomers and the isomer that crystallises preferentially may not be the dominant isomer in solution.

If we assume that, once an iron(II) complex has been formed with a tetradentate bis(pyridylmethyl) diamine ligand, the absolute configuration of the internal amine donors is fixed as being either *R* or *S* and only the triflate or acetonitrile co-ligands can dissociate and re-coordinate, a series of equilibria between six- and five-coordinated complexes can be proposed. In the case of a C_2-bridged ligand, the configuration at the amine N donor centres can in theory be either the same (*R*,*R* or *S*,*S*) or different (*R*,*S* or *S*,*R*) and the central five-membered chelate can adopt either a *twist* or an *envelope* (sometimes called *half chair*) conformation (Scheme 1).

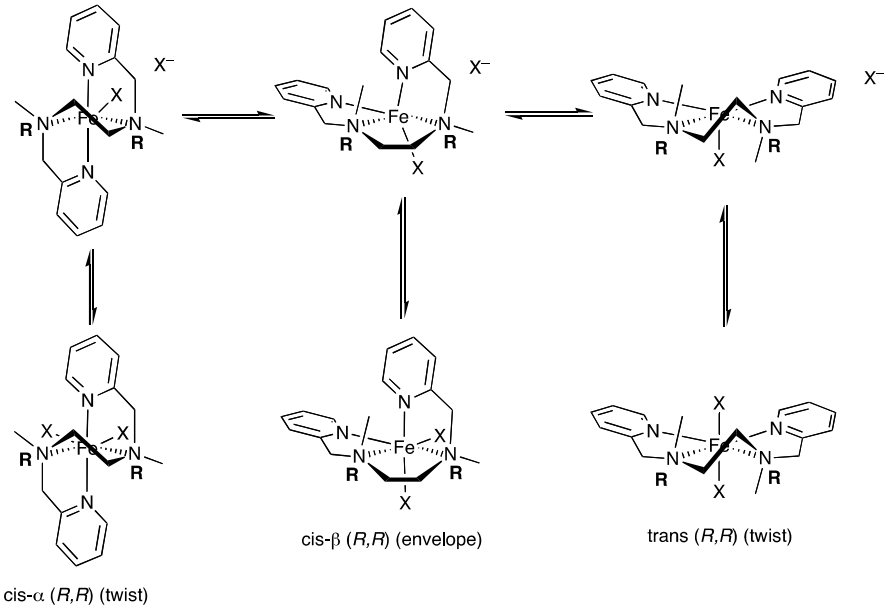

Scheme 1

In the case of complexes featuring BPMEN (**1**) or related ligands with three 5-membered chelate rings, the *cis*-α (*R*,*R* or *S*,*S*) geometry with a twist conformation of the central chelate ring is the only geometry seen in the solid state.[24, 41, 43-46] Loss of one of the weakly bound X ligands (for example OTf^- or CH_3CN) would result in a five-coordinate intermediate (Scheme 1). A clockwise twist of 120˚ around one of the N–Fe bonds and re-coordination of the X ligand would convert the *cis*-α (*R*,*R*) isomer into the *cis*-β (*R*,*R*) isomer with an envelope conformation of the central five-membered chelate ring. Another twist around the other N–Fe bond would give the *trans* (*R*,*R*) topology. These latter two ligand

rearrangements are highly unfavourable in the case of iron(II) complexes containing the BPMEN ligand due to the bite-angle strain.

^{19}F NMR spectroscopy

The ^{19}F NMR spectrum of [Fe(**1**)(OTf)$_2$] in CD_2Cl_2 solution consists of a single peak at -28 ppm at 298K, which shifts to -14 ppm at 188K due to Curie behaviour (Figure S10). This signal is assigned to a C_2-symmetric complex with a *cis*-α (*R,R* or *S,S*) coordination mode, which is the geometry found in the solid state structures of similar complexes such as [Fe(**1**)Cl_2][41] and which is generally the most stable geometry for tetradentate ligands featuring three 5-membered chelate rings.[42]

The ^{19}F NMR spectrum of the phenylene derivative [Fe(**2**)(OTf)$_2$] in CD_2Cl_2 at room temperature shows a sharp signal at -18 ppm and a broad resonance around -5 ppm. Upon cooling of this solution, the sharp signal shifts downfield, whereas the broad signal splits into 4 new resonances (see Figure 5). The sharp resonance at -18 ppm is assigned to the *cis*-α (*R,R* or *S,S*) geometrical isomer, based on its similarity with the previous complex [Fe(**1**)(OTf)$_2$] and because this is the geometry seen in the solid state structure (Figure 3). The broad signal is assigned to an interconverting mixture of the *cis*-β (*R,S* or *S,R*) and the *trans* (*R,S* or *S,R*) geometries, as shown in Scheme 2. This assignment is based on the similarity of the resolved signals at lower temperatures, with those observed for complexes [Fe(**3**)(OTf)$_2$] and [Fe(**4**)(OTf)$_2$], which consist predominantly as the *cis*-β and *trans* isomer, respectively (*vide infra*). The amount of *cis*-α isomer is about 40 % and the amounts of *cis*-β and *trans* isomers are approximately 20 % and 40 % respectively and this ratio does not appear to change significantly over the temperature range 298-198 K. As shown in Scheme 2, the *cis*-β (*R,S*) enantiomer can interconvert via the *trans* (*R,S*) isomer into its mirror image. The *trans* (*R,S*) isomer is identical to the *trans* (*S,R*) isomer and can thus be regarded as the meso form. This situation is akin to the stereochemistry of *cis*-1,2-dimethylcyclohexane, which in the planar representation appears as a meso form, but in the chair representation is actually a racemate whereby the enantiomers rapidly interconvert.

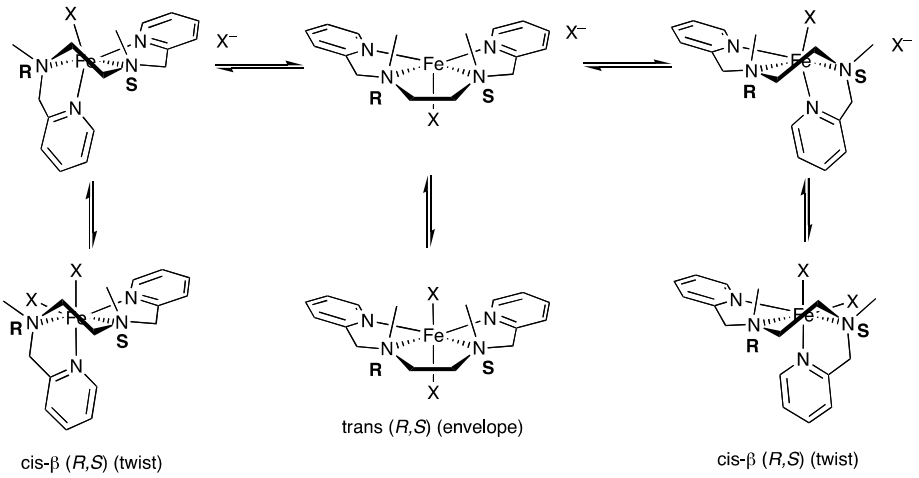

Scheme 2

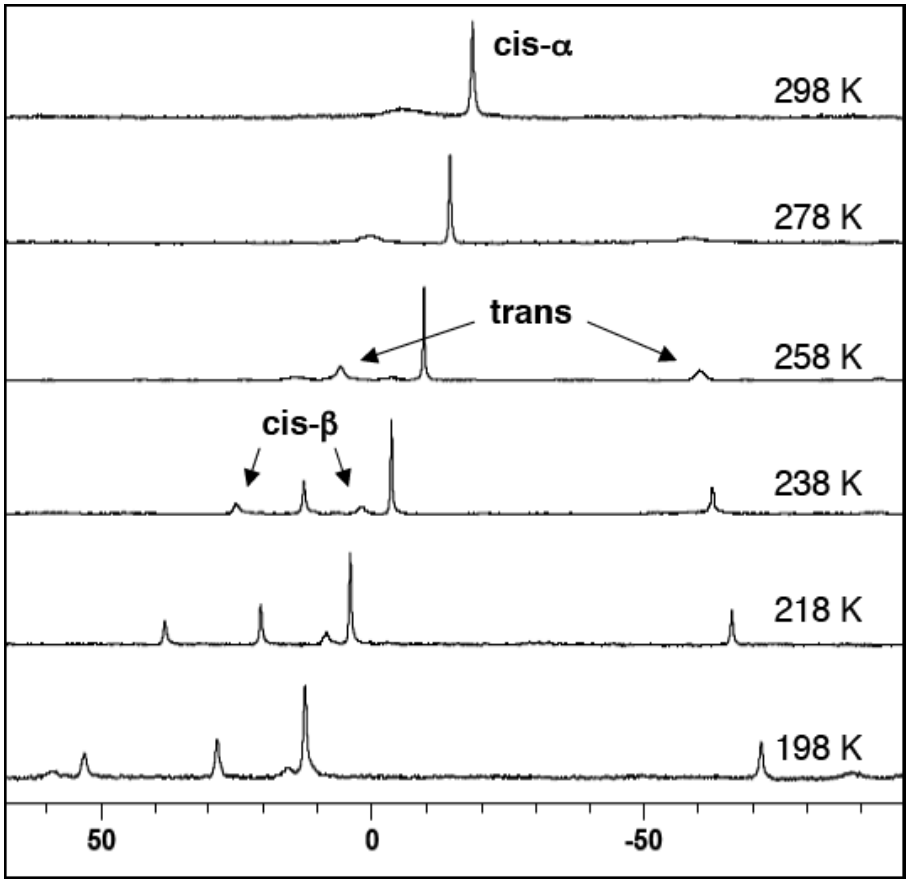

Figure 5. VT ^{19}F NMR spectra of complex [Fe(**2**)$(OTf)_2$] in CD_2Cl_2 between 198-298 K.

Both topological isomers, the *cis*-α(*R,R* or *S,S*) and the *cis*-β(*R,S* or *S,R*) geometry, of complex [Fe(**3**)$(OTf)_2$] have been separately prepared by Que and co-workers using two

different synthetic procedures.[33, 35] The *cis*-β (*R,S* or *S,R*) isomer was obtained by mixing equimolar amounts of the ligand BPMCN (**3**) and $Fe(OTf)_2 \cdot (CH_3CN)_2$ in THF,[34] whereas to obtain the *cis*-α (*R,R* or *S,S*) isomer, the dichloro complex [Fe(**3**)Cl_2] was first prepared by mixing the ligand with $FeCl_2$ in CH_3CN, followed by halide abstraction with AgOTf.[33] This interesting observation suggests that the nature of the counterions can control the binding of the ligand to the metal centre, to give either a *cis*-α topology where both amine nitrogens have the same absolute configuration (*R,R* or *S,S*) or a *cis*-β topology, where the absolute configurations are opposite (*R,S* or *S,R*). It is thus clear that these two isomers cannot interconvert. In this study, the complex [Fe(**3**)$(OTf)_2$] was prepared by mixing the ligand **3**, which was prepared from racemic *trans*-1,2-diaminocyclohexane, with $Fe(OTf)_2 \cdot (CH_3CN)_2$ in THF and this complex should therefore have the *cis*-β geometry. Indeed, the ^{1}H NMR spectrum in CD_3CN looks exactly like the previously reported spectrum by Que and co-workers,[33] showing 24 (12 pairs) of proton resonances due to the lack of symmetry of the *cis*-β geometry (see Figure S13). However, the ^{19}F NMR spectrum of this complex in CD_2Cl_2 solution at room temperature shows one very broad signal centred around -21 ppm (see Figure 6). Cooling this solution to 198 K reveals 6 peaks, which correspond to three isomers: the *cis*-β (*R,S* or *S,R*) isomer (ca. 56 %) which is in equilibrium with the *trans* (*R,S* or *S,R*) isomer (ca. 41 %) and the *cis*-β (*R,R* or *S,S*) isomer (ca. 3 %). A small amount of *cis*-α (*R,R* or *S,S*) isomer can be observed above 238 K, which converts to the *cis*-β (*R,R* or *S,S*) isomer at very low temperatures (see Scheme 1). The major *cis*-β (*R,S* or *S,R*) geometrical isomer is therefore not the only isomer in solution and, at least in CD_2Cl_2, is in equilibrium with the *trans* (*R,S* or *S,R*) isomer (see Scheme 2). It should be noted that because in the case of cis-β complexes, we are dealing with interconverting enantiomers with respect to the chirality at the N centres, the additional chirality in the case of complex [Fe(**3**)$(OTf)_2$] created by the racemic *trans*-cyclohexyldiamine unit at the two C centres therefore leads to an interconverting mixture of diastereomers, which may explain why only one set of signals is observed for the *cis*-β and the *trans* isomer.

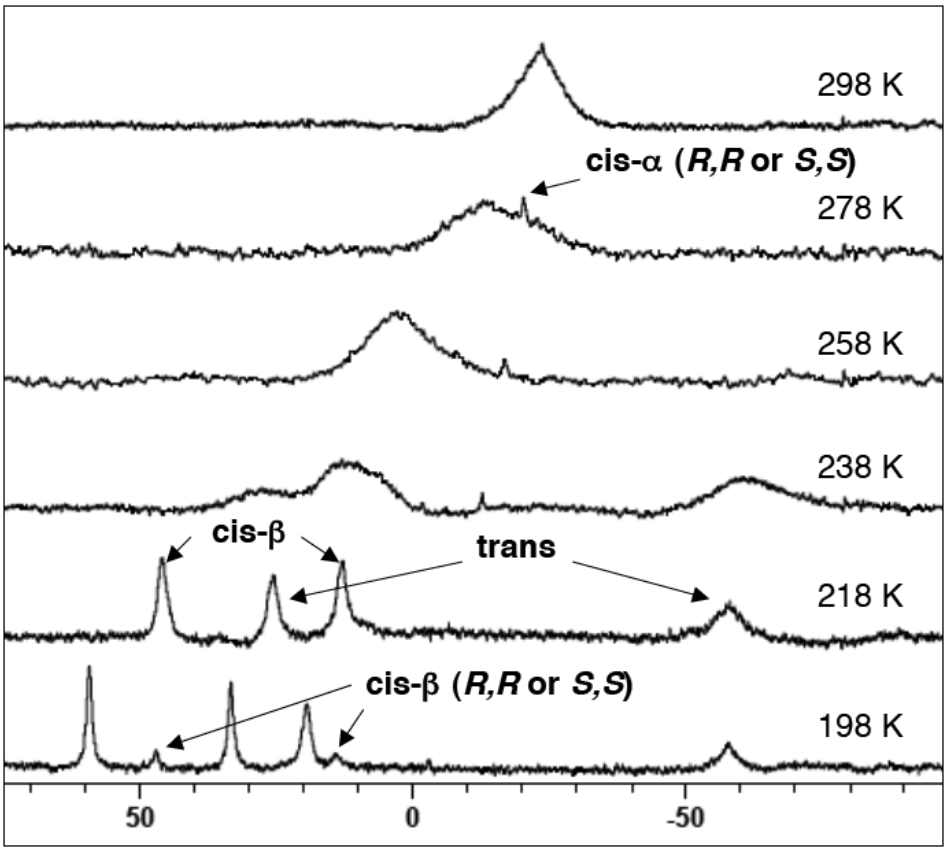

Figure 6. VT ^{19}F NMR spectra of complex [Fe(**3**)$(OTf)_2$] in CD_2Cl_2 between 198-298 K.

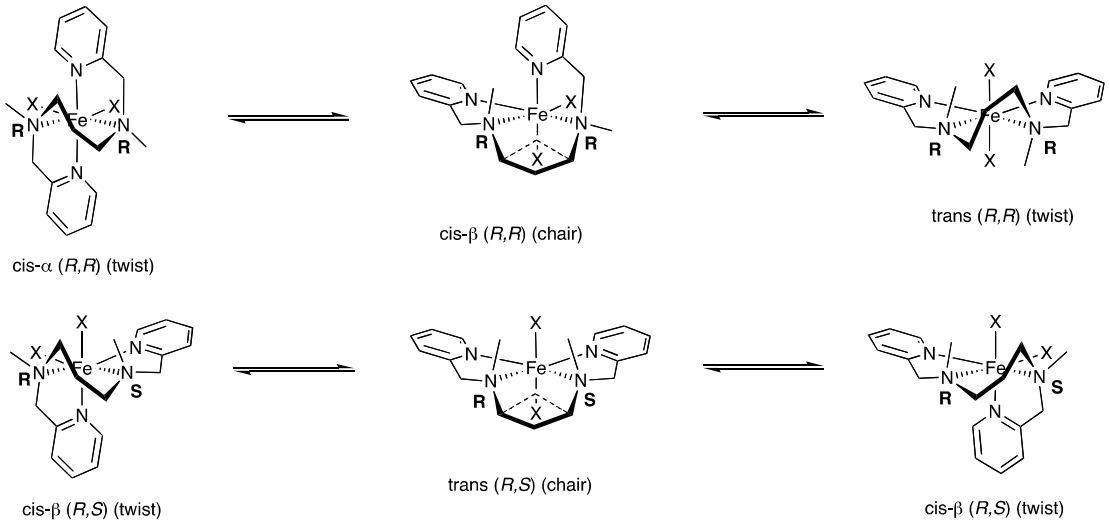

Scheme 3

As shown in Scheme 3, the central chelate in the propyl-bridged complex [Fe(**4**)$(OTf)_2$] forms a six-membered ring, which can adopt either a twist or a chair conformation (or the

less stable boat conformation, dashed line). The complexity and number of possible isomers has increased as *cis*-β (*R,R* or *S,S*) and *trans* (*R,R* or *S,S*) isomers are now more easily accessible. The order of relative stabilities of topological isomers of low spin Co(III) complexes containing the related 2,3,2-tet ligand is known to be as follows: *trans* (*R,S* or *S,R*) > *trans* (*R,R* or *S,S*) > *cis*-α (*R,R* or *S,S*) >> *cis*-β (*R,R* or *S,S*) and *cis*-β (*R,S* or *S,R*).[42] This order may be similar in the case of high spin Fe(II) complexes. Indeed, the X-ray analysis of complex [Fe(**4**)$(OTf)_2$], obtained from a CH_2Cl_2/pentane solution, shows the *trans* (*R,S*) geometry (see Figure S7). In addition, the *cis*-α (*R,R* or *S,S*) geometry has been previously observed in the solid state structure of the dichloro complex [Fe(**4**)Cl_2].[41] In CD_2Cl_2 solution, the ^{19}F NMR spectrum of [Fe(**4**)$(OTf)_2$] shows two broad resonances at room temperature, whereas at lower temperatures five peaks emerge, assumed to correspond to the *cis*-α isomer (ca. 2 %), a *cis*-β (*R,S* or *S,R*) isomer (ca. 16 %) and the major C_s symmetric *trans* (*R,S* or *S,R*) isomer (ca. 82 %) (see Figure S11). These spectra are identical to the ^{19}F NMR spectra observed by Que and co-workers.[37]

The butyl bridge in complex [Fe(**5**)$(OTf)_2$] generates a central seven-membered chelate ring, which has four possible conformers of which the twist-chair form is generally the most stable.[47] The ^{19}F NMR spectrum in CD_2Cl_2 solution at room temperature shows three broad peaks at -13, -22 and -42 ppm. At 218 K, five relatively sharp signals are observed, which have been tentatively assigned to the *trans* (*R,S* or *S,R*), *cis*-β (*R,S* or *S,R*) and *trans* (*R,R* or *S,S*) isomers (see Figure S12). The *trans* (*R,R* or *S,S*) isomer, which is C_2 symmetric gives rise to only one ^{19}F NMR signal. A related biphenyl-bridged complex, which also has a seven-membered central chelate ring, gives exclusively the *trans* (*R,R* or *S,S*) geometry.[48] The ^{19}F NMR spectrum shows a single peak at -11 ppm at 298K in this case, which shifts to +27 ppm at 198K.

In summary, the size and conformation of the central chelate ring formed by linear tetradentate bis(pyridylmethyl)diamine ligands, affects the flexibility of these ligands which can lead to more than one coordination geometry in solution. Due to the labile nature of high spin iron(II) complexes several equilibria can exist between different topological isomers. The ethylene-bridged BPMEN complex [Fe(**1**)$(OTf)_2$] gives exclusively the *cis*-α (*R,R* or *S,S*) geometry. The phenylene-bridged complex [Fe(**2**)$(OTf)_2$] consists of ca. 40 % *cis*-α

(*R*,*R* or *S*,*S*) isomer and 60 % *cis*-β (*R*,*S* or *S*,*R*) isomer which is in equilibrium with the *trans* (*R*,*S* or *S*,*R*) isomer. The cyclohexyl-bridged complex [Fe(**3**)$(OTf)_2$] prepared here is predominantly the *cis*-β (*R*,*S* or *S*,*R*) isomer, which is in equilibrium with the *trans* (*R*,*S* or *S*,*R*) isomer. In the case of the propyl-bridged complex [Fe(**4**)$(OTf)_2$], the *trans* (*R*,*S* or *S*,*R*) isomer is the major isomer, whereas the butyl-bridged complex [Fe(**5**)$(OTf)_2$] exists as a mixture of *trans* (*R*,*R* or *S*,*S*), *trans* (*R*,*S* or *S*,*R*) and *cis*-β (*R*,*S* or *S*,*R*) isomers.

Magnetic Susceptibilities

Magnetic susceptibility measurements have been used in this study to measure the relative ligand field strength of the different ligands **1** – **5** in octahedral iron(II) complexes. The magnetic moments of the iron(II) bis(triflate) complexes containing ligands **2** – **5**, measured in CD_3CN and CD_2Cl_2 solution at 298 K using the Evans' NMR method, are listed in Table 2 together with previously reported data for [Fe(**1**)$(OTf)_2$].[23] As expected from the weak ligand field exerted by triflate anions, CD_2Cl_2 solutions of all the bis(triflate) complexes display magnetic moments consistent with high-spin (HS) iron(II) (S = 2) centres. In CD_3CN solution, the triflate anions are displaced by stronger field acetonitrile ligands to yield dicationic complexes of the form $[Fe(L)(CH_3CN)_n]^{2+}$. In the case of L = **3**, **4** and **5**, the μ_{eff} values are consistent with high-spin iron(II) complexes at room temperature. In contrast, the μ_{eff} value measured for [Fe(**1**)$(OTf)_2$] and [Fe(**2**)$(OTf)_2$] at 298 K in CD_3CN were found to be lower than expected for a HS iron(II) centre, which is suggestive of the existence of spin crossover (SC) behaviour in these complexes.[49, 50]

Table 2. Selected physical data for complexes [Fe(**1**)$(OTf)_2$] – [Fe(**5**)$(OTf)_2$]

Complex	^{19}F in CD_3CN[a]		λ_{max}[b]	ε_{max}[b]	μ_{eff}[c]	μ_{eff}[c]
	δ (ppm)	$\nu_{1/2}$ (Hz)	(nm)	(M^{-1} cm^{-1})	CD_2Cl_2 (BM)	CD_3CN (BM)
[Fe(**1**)$(OTf)_2$]	-77	850	375	3800	5.27	4.26
[Fe(**2**)$(OTf)_2$]	-68	2150	366	2200	5.34	4.80
[Fe(**3**)$(OTf)_2$]	-67	340	376	1800	nd	5.01
[Fe(**4**)$(OTf)_2$]	-69	2100	341	770	nd	5.51
[Fe(**5**)$(OTf)_2$]	-68	2200	333	560	nd	5.40

[a] At 298K. [b] c = 0.5 mM in CH_3CN. [c] Evans' NMR method at 298K.

The magnetic behaviour of these iron(II) complexes in CD_3CN solution was further investigated by measurement of their magnetic moments over the temperature range 233-343 K using the Evans' NMR method (Figure 7). The magnetic moment of complex [Fe(**5**)$(OTf)_2$] (and also of complex [Fe(**4**)$(OTf)_2$], which is not shown for clarity) remains fully HS upon cooling to 233 K, whereas the magnetic moment of the phenylene derivative [Fe(**2**)$(OTf)_2$] decreases to μ_{eff} = 4.0 BM and of the cyclohexyl derivative [Fe(**3**)$(OTf)_2$] to μ_{eff} = 2.5 BM. Complex [Fe(**1**)$(OTf)_2$] undergoes a full spin transition within the temperature range, which shows a similar magnetic behaviour as the previously reported complex $[Fe(BPMEN)(CH_3CN)_2](ClO_4)_2$.[51]

The ^{19}F NMR analysis of CD_2Cl_2 solutions of the complexes has shown that all complexes except [Fe(**1**)$(OTf)_2$] exist as mixtures of isomers in solution. Such mixtures of isomers are likely to exist also in CD_3CN solutions and the magnetic moments determined in solution are therefore an average value of the various magnetic moments of the individual isomers. Notwithstanding, these magnetic moment measurements show clearly that the pyridylmethyl ligands that form exclusively 5-membered chelate rings upon coordination (BPMEN **1**, BPMPhN **2** and BPMCN **3**) exert a stronger ligand field than those that incorporate 6- or 7-membered chelate rings (BPMPN **4** and BPMBN **5**). The BPMEN ligand in complex [Fe(**1**)$(OTf)_2$], which gives rise to the cis-α isomer only, exerts the strongest ligand field. Ligands **2** and **3** result in complexes that are topological mixtures of isomers in solution, but with an average ligand field strength that is stronger than in the case of ligands **4** and **5**.

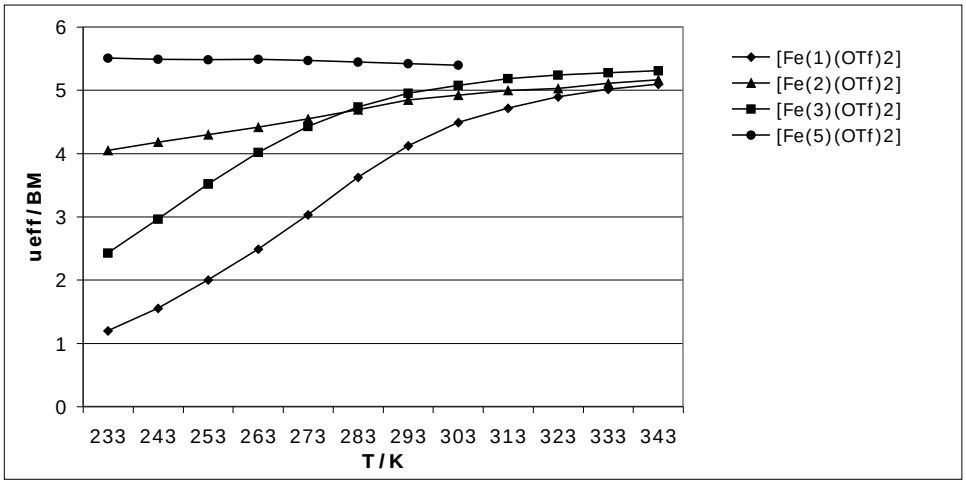

Figure 7. The magnetic moments of selected iron(II) complexes in CD_3CN solution as a function of temperature.

UV-Vis Spectroscopy

The UV-vis spectra of the iron(II) complexes of bis(pyridylmethyl)diamine ligands are dominated by high intensity bands in the UV region and broad transitions in the near-visible (Figure 8, Table 2). By analogy to spectra of similar iron(II) complexes of pyridine-alkylamino ligands, these two sets of bands can be assigned to ligand-centred π-π* transitions and MLCT bands between the iron(II) t_{2g} orbitals and the pyridine π*-orbitals, respectively.[52-55]

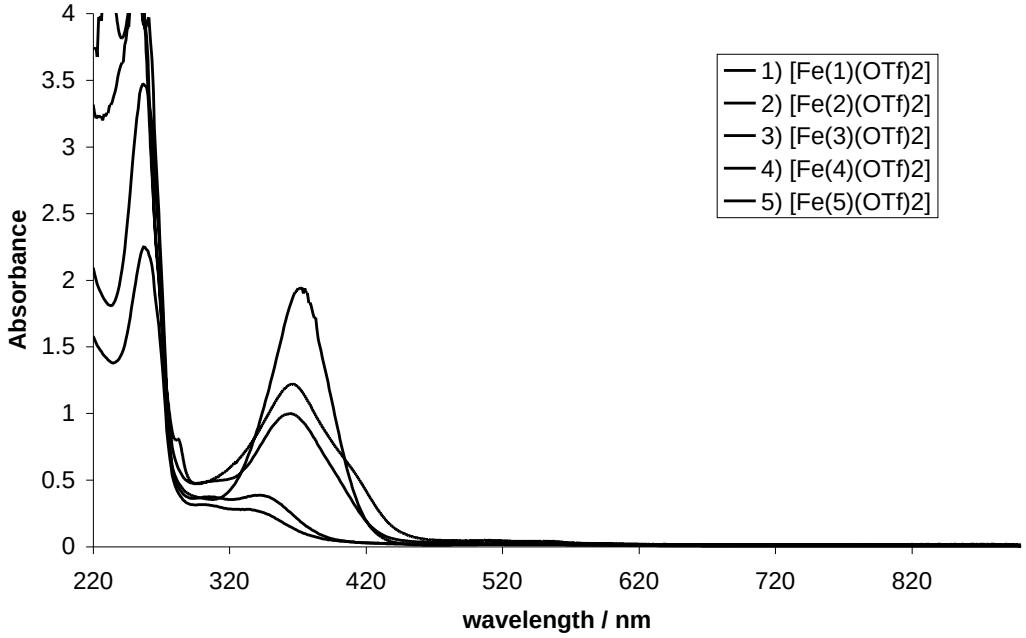

Figure 8. UV-vis spectra of iron bistriflate complexes of ligands **1** – **5** in CH_3CN (c = 0.5 mM).

One of the most noticeable facets of the UV-vis spectra in Figure 8 is that the extinction coefficient of the band of [Fe(**1**)$(OTf)_2$] centred at 375 nm (ε_{max} = 3800 M^{-1} cm^{-1}) is much larger than those of the other complexes. This presumably derives from the SC nature of this complex, which equates to an occupation of the low-spin configuration and results in an enhancement of the MLCT band.[56] As might be expected, a minor enhancement is also

observed for [Fe(**2**)$(OTf)_2$] and [Fe(**3**)$(OTf)_2$], which at room temperature show partial occupation of the low-spin configuration (see Figure 7).

It should be noted again, that except for complex [Fe(**1**)$(OTf)_2$], all complexes exist as a mixture of geometrical isomers in solution and the UV-vis spectra of these complexes consist therefore of several superimposed spectra, which makes correct peak assignments extremely difficult.

Catalytic Oxidation of Cyclohexane

The catalytic properties of the iron(II) bis(triflate) complexes containing ligands **1** – **5** for the oxidation of cyclohexane with H_2O_2 have been evaluated (Eq. 3).

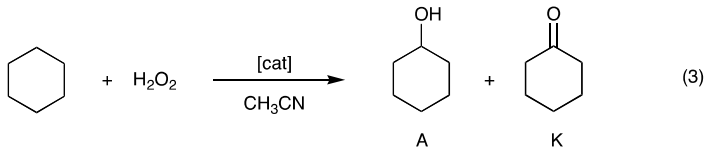

(3)

The oxidation reactions were carried out in acetonitrile as the solvent at room temperature (see Experimental Section). The H_2O_2 is added slowly during 25 minutes via a syringe pump to the reaction mixture, containing the solvent, cyclohexane (1000 equiv.) and the catalyst (1 equiv.). The addition of H_2O_2 is carried out slowly to avoid decomposition to water and dioxygen, although we have established that the rate of addition only marginally affects the conversion (see Figure S14). All the individual catalytic runs were performed at least twice. Two series of catalytic experiments were carried out initially, using 10 and 100 equiv. of H_2O_2. The amounts of cyclohexanol (A) and cyclohexanone (K) produced using the different catalysts are collected in Table 3. The iron bis(triflate) complex [Fe(**1**)$(OTf)_2$], containing the ligand BPMEN, is used as a benchmark against which the other catalysts are compared. We have previously reported that this catalyst, when using 10 equiv. of H_2O_2, converts 65% of the H_2O_2 added into oxygenated products, with a large ratio of cyclohexanol to cyclohexanone (A/K ratio) of 9.[23] These results are consistent with those reported previously by Que and co-workers for the complex [Fe(BPMEN)$(CH_3CN)_2$]$(ClO_4)_2$.[26]

Table 3. Results for the catalytic oxidation of cyclohexane.[a]

Run	Complex	Equiv. H_2O_2	A + K [b] (%)	A/K [c]
1[d]	[Fe(**1**)$(OTf)_2$]	10	65	9.5
2[d]	[Fe(**1**)$(OTf)_2$]	100	48	2.5
3	[Fe(**2**)$(OTf)_2$]	10	62	2.4
4	[Fe(**2**)$(OTf)_2$]	100	23	2.2
5	[Fe(**3**)$(OTf)_2$]	10	18	1.2
5a[e]	[Fe(**3**)$(OTf)_2$]	10	19	0.9
6	[Fe(**3**)$(OTf)_2$]	100	6	2.3
7	[Fe(**4**)$(OTf)_2$]	10	42	1.4
8	[Fe(**4**)$(OTf)_2$]	100	6	1.4
9	[Fe(**5**)$(OTf)_2$]	10	0	0
10	[Fe(**5**)$(OTf)_2$]	100	0.9	1.1

[a] Catalytic conditions: see Experimental Section. [b] Total percentage yield of cyclohexanol (A) + cyclohexanone (K), expressed as moles of product per mole of H_2O_2. [c] Ratio of moles of cyclohexanol (A) to moles of cyclohexanone (K). d Values from reference [23]. e Values from reference [33].

Increasing the amount of H_2O_2 to 100 equivalents leads to more oxidised product but, as can be seen in Table 3, this generally results in a lower percentage conversion of H_2O_2. The activity profile for the addition of up to 430 equivalents of H_2O_2 has been examined in more detail for complex [Fe(**1**)$(OTf)_2$] and the results are shown in Figure 9, where the number of equivalents of product is plotted *versus* the number of equivalents of H_2O_2 added. A dashed diagonal line is included to represent the total number of equivalents of oxidised product that can be obtained from any amount of H_2O_2 added. It appears that the addition of more H_2O_2 leads to more cyclohexanol (A) and cyclohexanone (K), but the relationship is far from linear. If we consider that a second equivalent of oxidant is required to oxidise cyclohexanol to cyclohexanone, the total conversion of H_2O_2 to generate the oxygenated products is given by the sum of the equivalents of cyclohexanol and twice the equivalents of cyclohexanone produced, which is the A+2K curve in Figure 9. Beyond approximately 100 equiv. of H_2O_2, the A+2K curve increases only marginally and falls continually further behind the theoretical maximum.

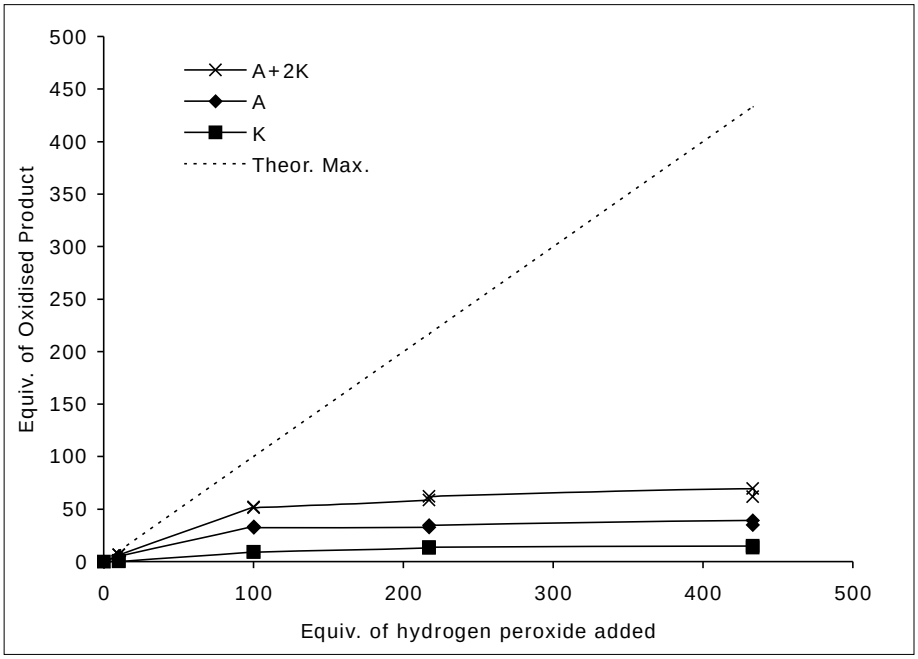

Figure 9. Product distribution as a function of the equivalents of hydrogen peroxide added. Conditions: catalyst: 2.1 µmol [Fe(**1**)OTf_2], 2.1 mmol cyclohexane (1000 equiv.), room temperature in acetonitrile. The dashed line represents the total number of equivalents of oxidised product that can be obtained.

In order to identify the differences in activity for the different catalysts, the activity profiles for all catalysts have been examined in more detail up to the addition of 50 equivalents of H_2O_2. The reaction profiles for the catalysts [Fe(**1**)$(OTf)_2$] and [Fe(**2**)$(OTf)_2$] are given in Figure 10 (the other profiles can be found in Figure S15).

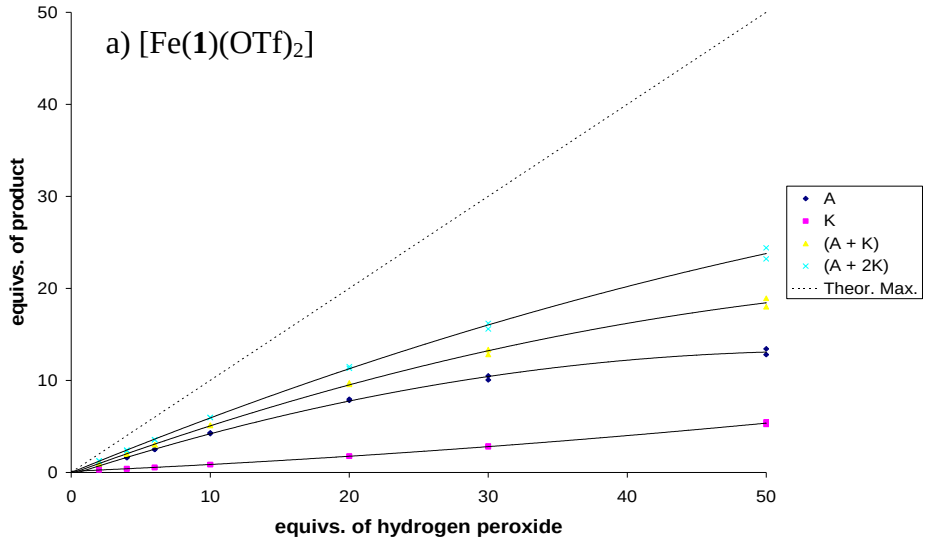

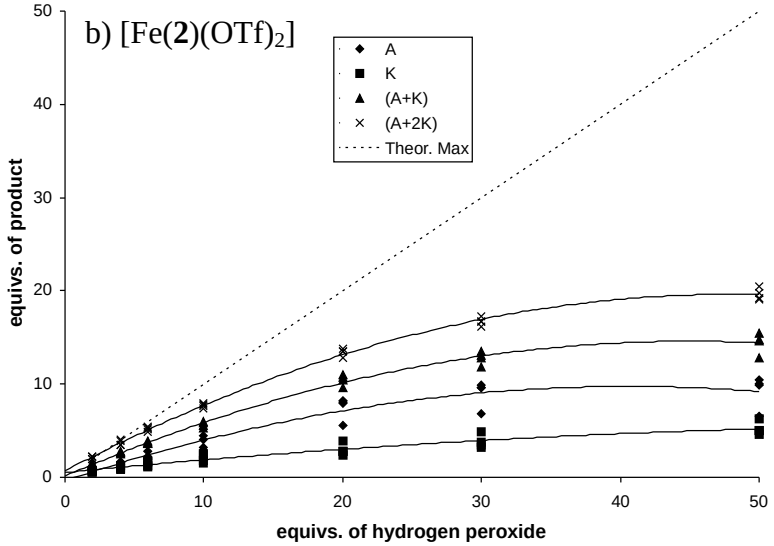

Figure 10. Product composition at various amounts of H_2O_2 in the oxidation of cyclohexane catalyzed by a) [Fe(**1**)(OTf)$_2$] and b) [Fe(**2**)(OTf)$_2$]. The dashed line represents the total number of equivalents of oxidised product that can be obtained.

Upon examining the reaction profile for [Fe(**1**)(OTf)$_2$] (Figure 10), it can be seen that the increase in production of cyclohexanol (A) observed upon the addition of increasing amounts of H_2O_2 deviates negatively from linearity, whereas the production of cyclohexanone (K) shows the opposite deviation (i.e. a decreasing A/K ratio). This is consistent with secondary oxidation of cyclohexanol to cyclohexanone, which increases in significance as the alcohol product builds up (*cf.* the decrease in A/K ratio from 9.5 to 2.5 observed upon moving from 10 to 100 equiv. of H_2O_2 in runs 1 and 2). Presumably, with further additions of oxidant, cyclohexanone would become the major product (A/K < 1). This over-oxidation process can be viewed as non-productive because it does not represent further conversion of cyclohexane to oxygenated product, which is reflected in the decrease in the percentage A+K yield observed upon moving from 10 to 100 equiv. H_2O_2 (runs 1 and 2) and the deviation of the A+K curve away from linearity in Figure 10.

In order to determine the efficiency of the various catalysts, the A+2K curves for the most active catalysts containing the ligands **1** – **4** have been determined and are collected in Figure 11. It can be seen that for complex [Fe(**1**)(OTf)$_2$] the A+2K curve is closest to the theoretical maximum (diagonal), which represents the highest conversion of H_2O_2 into oxidised

products. Complex [Fe(**2**)(OTf)$_2$] shows initially (<20 equiv. H_2O_2 added) a comparable catalytic activity, but levels off at higher conversions. Complex [Fe(**3**)(OTf)$_2$] shows a low catalytic activity, whereas complex [Fe(**4**)(OTf)$_2$] shows initially (<10 equiv. H_2O_2 added) a good performance, but this rapidly levels off. *It appears that for these catalysts the catalytic activity levels off at higher conversions due to catalyst deactivation and that this catalyst deactivation is related to the stability of the complexes under the oxidising conditions, which in turn is related to the coordination mode of the ligands.* Complex [Fe(**1**)(OTf)$_2$] contains the BPMEN ligand with a *cis-*α coordination geometry, which provides the strongest ligand field, as shown by magnetic susceptibility and UV-vis measurements. This complex is the most stable and most active catalyst for cyclohexane oxidation and only after the addition of approximately 100 equiv. of H_2O_2 does the catalytic activity start to level off, as shown in Figure 9. Complex [Fe(**2**)(OTf)$_2$], which only partially (ca. 40 %) exists as the *cis-*α isomer, is considerably less active. The other coordination geometries, *cis-*β and *trans,* result in weaker ligand fields and less active catalysts that deactivate more readily, as shown by the performance of complexes [Fe(**3**)(OTf)$_2$] and [Fe(**4**)(OTf)$_2$] (Figure 11).

Catalyst deactivation is a common but often overlooked problem in oxidation catalysis.[57] In heme-based oxidation catalysts, the mode of deactivation has been shown to involve oxidation of the porphyrin ligand.[58-61] The exact deactivation pathway of the non-heme catalysts studied here is not known at this stage. However, based on the results presented here and recent observations of the oxidation of (pyridylmethyl)amine type ligands,[62, 63] we believe that oxidative degradation of the ligand is the main pathway for catalyst deactivation. The reason why iron catalysts containing ligands **2 – 5** deactivate more rapidly is that these complexes exist mostly as kinetically labile high spin *cis-*β or *trans* complexes at room temperature in acetonitrile, whereas the *cis-*α complex [Fe(**1**)(OTf)$_2$] exists at least partly as a kinetically inert low spin complex. We are currently investigating the mechanism of this deactivation pathway with the aim to improve the stability and efficiency of these oxidation catalysts.

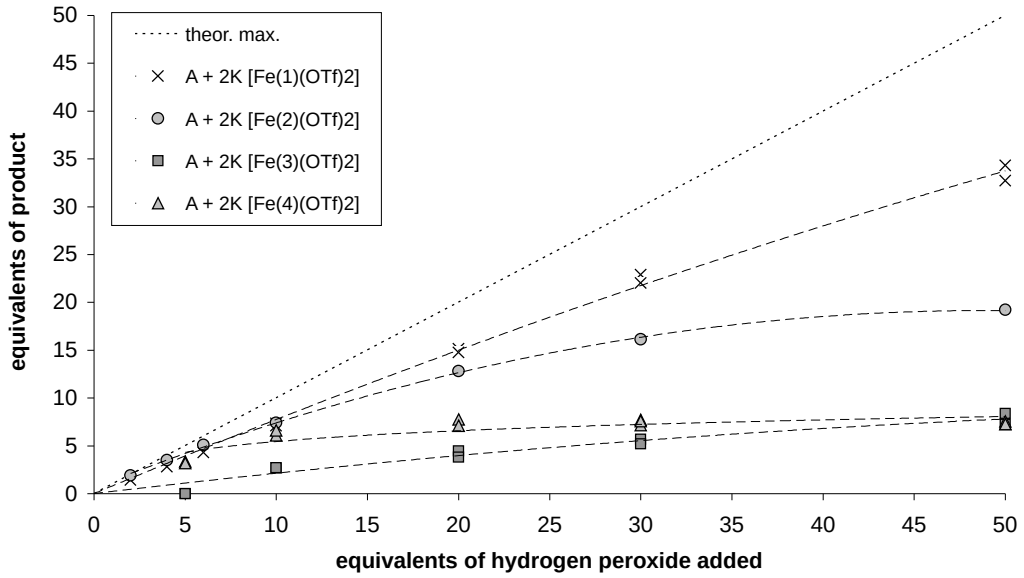

Figure 11. Conversion of H_2O_2 into oxygenated products (A+2K curves) for different catalysts. The dashed line represents the total number of equivalents of oxidised product that can be obtained.

Conclusions

A series of iron(II) bis(triflate) complexes featuring bis(pyridylmethyl)diamine ligands **1** – **5**, containing different backbones with various degrees of flexibility, has been prepared and characterised. The coordination geometries of these complexes have been determined both in the solid state and in solution by ^{19}F NMR and these studies have shown that only the BPMEN ligand **1** results in a single isomer of complex [Fe(**1**)$(OTf)_2$], containing the *cis*-α coordination geometry which, according to magnetic susceptibility measurements has the strongest ligand field. All the other ligand backbones in the complexes of ligands **2** – **5** result in various amounts of other coordination geometries (*cis*-β or *trans*), which generally show a lower ligand field strength. The catalytic acitiy of the complexes as catalysts for the oxidation of cyclohexane using H_2O_2 as the oxidant has been investigated. The changes in product distribution during the addition of the oxidant to the substrate have been determined for all catalysts and complex [Fe(**1**)$(OTf)_2$] was found to be the most productive catalyst amongst the series studied here. The better performance of this catalysts compared to the other catalysts is believed to be due to the higher stability and the lifetime of this particular

catalysts under the harsh oxidising conditions. Oxidation of the ligand is believed to be the main source of catalyst degradation.

Experimental

General

All moisture and oxygen sensitive compounds were prepared using standard high vacuum line, Schlenk, or cannula techniques. A standard nitrogen-filled glove box was used for any subsequent manipulation and storage of these compounds. Standard ^{1}H, ^{19}F and ^{13}C NMR spectra were recorded using a Bruker AC-250 MHz spectrometer. VT-NMR spectra were recorded using a Bruker AM-500 MHz or a DRX-400 MHz spectrometer. The ^{1}H and ^{13}C NMR chemical shifts were referenced to the residual protio impurity and ^{13}C NMR signal of the deuterated solvent, respectively. The ^{19}F NMR chemical shifts were referenced to $CFCl_3$. Mass spectra were recorded using either a VG Autospec or a VG Platform II spectrometer. Elemental analyses were performed by the Science Technical Support Unit at The London Metropolitan University. GC analysis was performed using an Agilent 6890A gas chromatograph on either a HP-5 (30 m x 0.32 mm, film thickness 0.25 μm) or an Innowax (30 m x 0.25 mm, film thickness 0.25 μm) column. Toluene was used as the standard for quantitative analysis and product identities were confirmed using GC-MS. UV-vis spectra were recorded at 298K in acetonitrile solution using a Perkin-Elmer Lambda 20 spectrometer.

Solvents and Reagents

Diethyl ether and tetrahydrofuran were dried by prolonged reflux, under a nitrogen atmosphere, over sodium metal with a benzephenone ketyl indicator and distilled freshly prior to use. Dichloromethane and acetonitrile were treated in a similar manner, but using calcium hydride as the drying agent. Toluene and pentane were dried by passing through a column, packed with commercially available Q-5 reagent (13 % CuO on alumina) and activated alumina (pellets, 3 mm), in a stream of nitrogen. The synthesis and characterisation of the following compounds has been reported previously: $[Fe(OTf)_2(CH_3CN)_2]$,[64] $[Fe(\mathbf{1})(OTf)_2]$,[23] $[Fe(\mathbf{3})(OTf)_2]$[33] and $[Fe(\mathbf{4})(OTf)_2]$[37]. The ligands and ligand precursors N,N'-dimethyl-N,N'-bis(2-pyridylmethyl)cyclohexyl diamine (**3**),[35] N,N'-dimethyl-N,N'-bis(2-pyridylmethyl)propyl diamine (**4**)[38] and N,N'-bis(2-pyridylmethyl)butylene diamine[39]

were prepared according to published procedures. The ligand N,N'-dimethyl-N,N'-bis(2-pyridylmethyl)cyclohexyl diamine (**3**) was prepared from racemic *trans*-1,2-diaminocyclohexane.

Synthesis of Ligands and Complexes

4,5-dichloro-1,2-bis(2-pyridylmethylamino)benzene Pyridine-2-carboxaldehyde (2.15 mL, 22.6 mmol) was added to a mixture of 4,5-dichloro-1,2-diaminobenzene (1.00 g, 5.65 mmol) and sodium tri(acetoxy)borohydride (6.23 g, 29.4 mmol) in dichloromethane (DCM) (150 mL), and the reaction was left to stir for 48 hours. Subsequent to this period, 50 mL of 3M aqueous sodium hydroxide solution was added and the stirring continued for a further 30 minutes. The organic layer was separated and the aqueous layer extracted with DCM (2 x 100 mL). All the organic fractions were combined, dried ($MgSO_4$) and all volatiles removed. Trituration of the residue in ethanol, followed by air drying gave a yellow feathery solid (1.52 g, 74.9 %). ^{1}H-NMR (d_6-DMSO): δ 8.54 (d, 2H, *J* = 4.7Hz, 6-Py*H*), 7.75 (dt, 2H, *J* = 7.7Hz, *J* = 1.6Hz, 4-Py*H*), 7.37 (d, 2H, *J* = 7.7Hz, 3-Py*H*), 7.26 (dd, 2H, *J* = 7.0Hz, *J* = 5.2Hz, 5-Py*H*), 6.42 (s, 2H, Ph*H*), 5.93 (t, 2H, *J* = 5.6Hz, N*H*), 4.41 (d, 4H, *J* = 5.5Hz, NCH_2). ^{13}C-NMR (d_6-DMSO): δ 158.7 (*ipso*), 148.9, 136.7, 136.1, 122.2, 121.4, 118.1, 110.3, 48.2 (NCH_2). MS (+ EI): *m/z* (%) 358 (24) [M^+], 278 (8) [$(M\text{-}PyH_2)^+$], 266 (20) [$(M\text{-}PyCH_2)^+$], 187 (32) [$(M\text{-}(PyH)(PyCH_2))^+$], 93 (99) [$(PyCH_3)^+$], 80 (100) [$(PyH_2)^+$]. Anal. Calcd. (found) for $C_{18}H_{16}Cl_2N_4$: C, 60.18 (59.93); H, 4.49 (4.29); N, 15.60 (15.79).

4,5-dichloro-1,2-bis[methyl(2-pyridylmethyl)amino]benzene (**2**)

n-Butyl lithium (4.90 mL of 1.6M in hexanes, 7.79 mmol) was added dropwise to a solution of 4,5-dichloro-1,2-bis(2-pyridylmethylamino)benzene (1.40 g, 3.90 mmol) in THF (75 mL), precooled to -78°C. The mixture was stirred at -78 ˚C for 1 hour followed by a further hour at room temperature to give a dark red-brown solution. This was cooled to -78°C and methyl iodide (2.43 mL, 39.0 mmol) was added, after which the cooling bath was removed and the reaction mixture stirred for a further 12 hours. Subsequent to this period, saturated aqueous sodium hydrogen carbonate solution and diethyl ether was added. Separation of the organic layer was followed by extraction of the aqueous layer with DCM (2x100 mL). The organic fractions were combined, dried ($MgSO_4$) and the solvent removed using the rotary evaporator. The resultant residue was extracted with diethyl ether and the

extract reduced to dryness to give a yellow viscous oil that solidifies to a waxy solid upon prolonged standing (1.16 g, 76.9 %). ^{1}H-NMR ($CDCl_3$): δ 8.53 (d, 2H, *J* = 4.8Hz, 6-Py*H*), 7.52 (dt, 2H, *J* = 7.6Hz, *J* = 1.7Hz 4-Py*H*), 7.13 (dd, 2H, *J* = 6.9Hz, *J* = 5.0Hz, 5-Py*H*), 7.03 (d, 2H, *J* = 7.7Hz , 3-Py*H*), 6.95 (s, 2H, Ph*H*), 4.56 (s, 4H, NCH_2), 2.78 (s, 6H, N*Me*). ^{13}C-NMR ($CDCl_3$): δ 157.7 (*ipso)*, 148.6, 143.4, 135.8, 124.5, 122.1, 121.5, 120.8, 58.6 (NCH_2), 39.3 (N*Me*). MS (+EI): *m/z* (%) 386 (29) [M^+], 294 (55) [(M-PyCH_2)$^+$], 215 (85) [(M-(PyH)(PyCH_2))$^+$], 201 (56) [(M-(PyCH_3)(PyCH_2))$^+$], 183 (45), 93 (100) [(PyCH_3)$^+$].

N,N'-dimethyl-N,N'-bis(2 pyridylmethyl)butylene diamine (**5**)

N,N'-bis(2-pyridylmethyl)butylene diamine (8.10 g, 30 mmol) was heated under reflux with formic acid (70 mL) and formaldehyde (70 mL) for 24 hours. The product was cooled in an ice bath. The solution was made alkaline by saturated sodium hydroxide and the solution was extracted with chloroform (3 x 75 mL). The organic fractions were combined and dried over $MgSO_4$, filtered and all volatiles removed on the rotary evaporator to give a yellow-brown oil. Part of this product (2.61 g, 8.76 mmol) was purified by the addition of 1 equivalent of oxalic acid (0.79 g, 8.76 mmol) in methanol (25 mL) added to the yellow-brown oil with stirring to afford a white precipitate. This was isolated by filtration, washed with small amounts of cold methanol and air dried. This was treated with 3 M sodium hydroxide and extracted with dichloromethane (3 x 25 mL). The organic fractions were combined and dried over magnesium sulphate, filtered and all volatiles removed on the rotary evaporator to give a brown oil (0.75 g, 2.52 mmol, 29%). ^{1}H NMR ($CDCl_3$): δ 8.46 (dd, 2H, *J* = 1 Hz, *J* = 4.9 Hz, PyH_α), 7.56 (dt, 2H, *J* = 1.8 Hz, *J* = 7.7 Hz, PyH_β), 7.35 (d, 2H, *J* = 7.8 Hz, PyH_β), 7.07 (ddd, 2H, *J* = 1 Hz, *J* = 5.0 Hz, *J* = 7.7 Hz, PyH_γ), 3.57 (s, 4H, NCH_2Py), 2.36 (t, 4H, *J* = 6.8 Hz, NCH_2), 2.17 (s, 6H, CH_3), 1.49 (q, 4H, *J* = 3.4 Hz, CH_2). ^{13}C NMR ($CDCl_3$): δ 160, 149, 137, 123, 122, 63.9, 57.6, 42.4, 25.1. MS (EI): *m/z* (%) 298 (30) [M^+], 206 (40) [M – (CH_2Py)].

Synthesis of metal complexes

The iron(II) bis(triflate) complexes [Fe(**1**)$(OTf)_2$], [Fe(**3**)$(OTf)_2$] and [Fe(**4**)$(OTf)_2$] were prepared by mixing [Fe$(OTf)_2(CH_3CN)_2$] and the appropriate ligand in THF at room temperature. The first two complexes precipitated after one day, whereas several days were

required for the third complex. In all cases, the mixture was filtered and the residue was washed with diethylether and dried in vacuo. The spectroscopic details were identical to those previously reported for [Fe(**1**)$(OTf)_2$],[23] [Fe(**3**)$(OTf)_2$][35] and [Fe(**4**)$(OTf)_2$].[37]

[Fe(**2**)$(OTf)_2$]: A solution of the ligand (1.09 g, 2.81 mmol) in THF (50 mL) was added to a stirring solution of [Fe$(OTf)_2(CH_3CN)_2$] (1.12 g, 2.56 mmol) in THF (50 mL). A precipitate began to form within minutes. After stirring overnight, the volume of THF was reduced to approximately 10 mL and the reaction mixture filtered. The solid obtained was washed with multiple small quantities of THF to remove green impurities, followed by a single washing with diethyl ether (75 mL) and dried under vacuum to give the product as a white powder (1.46 g, 77.2 %). ^{1}H-NMR (CD_3CN): δ 123.2 (2H, PyH_α), 72.3 (6H, N*Me*), 55.5 (2H, PyH_β), 54.3 (2H, Py$H_{\beta'}$), 32.3 (2H, CH_{2A}), 26.4 (2H, CH_{2B}), 18.8 (2H, PyH_γ), 7.0 (2H, Ph*H*). ^{19}F-NMR (CD_2Cl_2): δ -19.9. ^{19}F-NMR (CD_3CN): δ -68.1. MS (+ FAB): *m/z* 1332 ([2M-OTf]$^+$), 740 ([M]$^+$), 591 ([M-OTf]$^+$). Anal. Calcd. (found) for $C_{22}H_{20}Cl_2F_6FeN_4O_6S_2$: C, 35.65 (35.87); H, 2.72 (2.75); N, 7.56 (7.41). μ_{eff} (CD_2Cl_2) = 5.34 μ_B. μ_{eff} (CD_3CN) = 4.80 μ_B.

Crystal data for [Fe(**2**)$(OTf)_2$]: $C_{22}H_{20}Cl_2F_6FeN_4O_6S_2$, M = 741.29, monoclinic, $P2_1/c$ (no. 14), a = 15.1625(11), b = 23.9862(17), c = 15.8454(18) Å, β = 93.649(8)°, V = 5751.1(9) Å^3, Z = 8 (2 independent molecules), D_c = 1.712 g cm^{-3}, μ(Mo-Kα) = 0.940 mm^{-1}, T = 173 K, yellow blocks, Oxford Diffraction Xcalibur 3 diffractometer; 17726 independent measured reflections, F^2 refinement, R_1 = 0.048, wR_2 = 0.120, 12074 independent observed absorption-corrected reflections [$|F_o| > 4\sigma(|F_o|)$, $2\theta_{max}$ = 64°], 921 parameters. CCDC 618854.

[Fe(**5**)$(OTf)_2$]: The ligand **5** (0.25g, 0.839mmol) and [Fe$(OTf)_2(CH_3CN)_2$] (0.37g, 0.839mmol) were stirred together in THF for 3 weeks. The off-white precipitate formed was filtered, washed with dry diethyl ether and dried in vacuo to give the product as an off-white solid (0.19g, 35 %). ^{1}H-NMR (CD_3CN): δ 120 (2H, PyH_α), 102.3 (4H, CH_2), 83.1 (4H, CH_2), 69.1 (2H, PyH_β), 66.3 (2H, Py$H_{\beta'}$), 50.1 (2H, CH_{2A}Py), 46.7 (6H, N*Me*), -5.1 (2H, CH_{2B}Py), -26.4 (2H, PyH_γ). ^{19}F-NMR (CD_2Cl_2, 298K): δ -12, -22, -42. ^{19}F-NMR (CD_3CN, 298K): δ -67.8. MS (+FAB): *m/z* (%) 503 (10) [M$^+$ - (OTf)]. Anal. calc. (found) for $C_{20}H_{26}N_4FeO_6S_2F_6$: C, 36.82 (36.70); H, 4.02 (3.94); N, 8.59 (8.46).

Standard Testing Conditions for the Oxidation of Cyclohexane.

Catalytic oxidations were all run at room temperature. The reaction products were analysed by GC analysis, using GC-MS for product identification. All catalytic data quoted is the average of at least two runs. 2.1 mmol (0.23 mL) of cyclohexane was added to a 75x25 mm sample vial containing 2.1 μmol of complex dissolved in 2.7 mL of acetonitrile and a small egg-shaped stirrer bar, and the mixture stirred until the substrate had fully dissolved. For the addition of 10 equivalents of H_2O_2 (relative to the amount of catalyst), 0.3 mL of 70 mM solution of hydrogen peroxide in acetonitrile was added dropwise over the course of 25 minutes, using a syringe pump. Upon completion of addition, the solution was stirred for a further 15 minutes and subsequently filtered through a pad of silica to remove the catalyst. The silica was then washed with 3.0 mL of acetonitrile and the washings combined with the filtered reaction mixture. The final concentration of the components in the reaction mixture was: cyclohexane = 700 mM, H_2O_2 = 7mM and catalyst = 0.7 mM. This gave a substrate: oxidant: catalyst molar ratio of 1000: 10: 1. Other ratios between H_2O_2 and catalyst were obtained by adding different amounts of H_2O_2.

The acetonitrile solutions of hydrogen peroxide were prepared from commercially available 35 % aqueous hydrogen peroxide and reagent grade acetonitrile. The resultant acetonitrile solution was used without drying. The silica pads used for catalyst removal were prepared by inserting a glass wool plug into a Pasteur pipette, onto which an approximately 25 mm deep layer of silica was added.

Supporting Information

The supplementary crystallographic data for this paper can be obtained free of charge via www.ccdc.cam.ac.uk/conts/retrieving.html (or from the Cambridge Crystallographic Data Centre, 12 Union Road, Cambridge CB2 1EZ, UK; fax: (+44) 1223-336-033; or deposit@ ccdc.cam.ac.uk). The Supporting information also contains VT-^{19}F NMR spectra and cyclohexane oxidation results.

Acknowledgements

We are grateful to EPSRC and BP Chemicals Ltd. for a CASE award to J.E. We also thank the British Council and IAESTE UK for organising the training placement for M.B.

Mr. Richard Sheppard and Mr. Peter Haycock are thanked for their assistance in NMR measurements.

References

1. R.A. Sheldon, J.K. Kochi, *Metal-catalysed oxidations of organic compounds*. Academic Press: New York, **1981**.
2. A.E. Shilov, G.B. Shul'pin, *Activation of catalytic reactions of saturated hydrocarbons in the presence of metal complexes*. Kluwer: Dordrecht, **2000**.
3. J.A. Labinger, *J. Mol. Catal.* **2004,** 220, 27-35.
4. S.S. Stahl, J.A. Labinger, J.E. Bercaw, *Angew. Chem. Int. Ed. Engl.* **1998,** 37, 2180-2192.
5. B. Meunier, S.P. de Visser, S. Shaik, *Chem. Rev.* **2004,** 104, 3947-3980.
6. I.V. Kozhevnikov, *Catalysis by Polyoxometalates*. Wiley: Chichester, **2002**; Vol. 2.
7. C.L. Hill, C.M. Prosser-McCartha, *Coord. Chem. Rev.* **1995,** 143, 407.
8. N. Mizuno, M. Misono, *Chem. Rev.* **1998,** 98, 199-218.
9. R. Curci, L. D'Accolti, C. Fusco, *Acc. Chem. Res.* **2006,** 39, 1-10.
10. P.R. Schreiner, A.A. Fokin, *Chem. Rec.* **2004,** 3, 247-257.
11. X. Tong, J. Xu, H. Miao, *Adv. Synth. Catal.* **2005,** 347, 1953-1957.
12. R.H. Holm, J.P. Donahue, *Polyhedron* **1993,** 12, 571-589.
13. C.W. Jones, *Applications of Hydrogen Peroxide and Derivatives*. The Royal Society of Chemistry: Cambridge, **1999**.
14. C.L. Hill, *Nature* **1999,** 401, 436-437.
15. S. Tanase, E. Bouwman, *Adv. Inorg. Chem.* **2006,** 58, 29-75.
16. M. Costas, K. Chen, L. Que Jr., *Coord. Chem. Rev.* **2000,** 200-202, 517-544.
17. B. Meunier, *Biomimetic Oxidations Catalyzed by Transition Metal Complexes*. Imperial College Press: London, **2000**.
18. M.M. Abu-Omar, A. Loalza, N. Hontzeas, *Chem. Rev.* **2005,** 105, 2227-2252.
19. M. Costas, M.P. Mehn, M.P. Jensen, L. Que Jr., *Chem. Rev.* **2004,** 104, 939-986.
20. C. Walling, *Acc. Chem. Res.* **1975,** 8, 125-131.
21. J. Kim, R.G. Harrison, C. Kim, L. Que Jr., *J. Am. Chem. Soc.* **1996,** 118, 4373-4379.
22. M.H. Lim, J.-U. Rohde, A. Stubna, M.R. Bukowski, M. Costas, R.Y.N. Ho, E. Münck, W. Nam, L. Que Jr., *PNAS* **2003,** 100, 3665-3670.
23. G.J.P. Britovsek, J. England, A.J.P. White, *Inorg. Chem.* **2005,** 44, 8125-8134.

24. K. Chen, L. Que Jr., *Chem. Commun.* **1999**, 1375-1376.

25. J. England, G.J.P. Britovsek, N. Rabadia, A.J.P. White, *Inorg. Chem.* **2007,** 46, 3752-3767.

26. K. Chen, L. Que Jr., *J. Am. Chem. Soc.* **2001,** 123, 6327-6337.

27. S.V. Kryatov, E.V. Rybak-Akimova, S. Schindler, *Chem. Rev.* **2005,** 105, 2175-2226.

28. K. Chen, M. Costas, L. Que Jr., *Dalton Trans.* **2002**, 672-679.

29. A. Bassan, M.R.A. Blomberg, P.E.M. Siegbahn, L. Que Jr., *Chem. Eur. J.* **2005,** 11, 692-705.

30. W. Nam, *Acc. Chem. Res.* **2007,** 40, 522-531.

31. L. Que Jr., *Acc. Chem. Res.* **2007,** 40, 493-500.

32. J.T. Groves, *J. Chem. Educ.* **1985,** 62, 928-931.

33. M. Costas, L. Que Jr., *Angew. Chem. Int. Ed.* **2002,** 41, 2179-2181.

34. M. Costas, J.-U. Rohde, A. Stubna, R.Y.N. Ho, L. Quaroni, E. Münck, L. Que Jr., *J. Am. Chem. Soc.* **2001,** 123, 12931-12932.

35. M. Costas, A. Tipton, K. Chen, D.-H. Jo, L. Que Jr., *J. Am. Chem. Soc.* **2001,** 123, 6722-6723.

36. M. Fujita, L. Que Jr., *Adv. Synth. Catal.* **2004,** 346, 190-194.

37. R. Mas-Ballesté, M. Costas, T. van den Berg, L. Que Jr., *Chem. Eur. J.* **2006,** 12, 7489-7500.

38. C.-M. Che, W.-T. Tang, C.-K. Li, *J. Chem. Soc., Dalton Trans.* **1990**, 3735-3739.

39. G. Anderegg, N.G. Podder, P. Bläuenstein, M. Hangartner, H. Stünzi, *J. Coord. Chem.* **1975,** 4, 267-275.

40. S. Miyano, A. Uno, N. Abe, *Chem. Pharm. Bull.* **1967,** 14, 515.

41. N. Raffard, V. Balland, A.J. Simaan, S. Létard, M. Nierlich, K. Miki, F. Banse, E. Anxolabéhère-Mallart, J.-J. Girerd, *C. R. Acad. Sci. (Paris) Ser. C* **2002,** 5, 99-109.

42. A.L. Gavrilova, B. Bosnich, *Chem. Rev.* **2004,** 104, 349-383.

43. Y. Mekmouche, S. Ménage, J. Pécaut, C. Lebrun, L. Reilly, V. Schuenemann, A. Trautwein, M. Fontecave, *Eur. J. Inorg. Chem.* **2004**, 3163-3171.

44. B. Rieger, A.S. Abu-Surrah, R. Fawzi, M. Steiman, *J. Organomet. Chem.* **1995,** 497, 73-79.

45. J. Simaan, S. Poussereau, G. Blondin, J.-J. Girerd, D. Defaye, C. Philouze, J. Guilhem, L. Tchertanov, *Inorg. Chim. Acta* **2000,** 299, 221-230.

46. M.C. White, A.G. Doyle, E.N. Jacobsen, *J. Am. Chem. Soc.* **2001,** 123, 7194-7195.

47. M. Christl, J.D. Roberts, *J. Org. Chem.* **1972,** 37, 3443-3452.

48. G.J.P. Britovsek, J. England, A.J.P. White, *Dalton Trans.* **2006**, 1399-1408.

49. P. Gütlich, Y. Garcia, H.A. Goodwin, *Chem. Soc. Rev.* **2000,** 29, 419-427.

50. H. Toftlund, J.J. McGarvey, *Top. Curr. Chem.* **2004,** 233, 151-166.

51. K.P. Bryliakov, E.A. Duban, E.P. Talsi, *Eur. J. Inorg. Chem.* **2005**, 72-76.

52. V. Balland, F. Banse, E. Anxolabéhère-Mallart, M. Nierlich, J.-J. Girerd, *Eur. J. Inorg. Chem.* **2003**, 2529-2535.

53. A.S. Borovik, V. Papaefthymiou, L.F. Taylor, O.P. Anderson, L. Que Jr., *J. Am. Chem. Soc.* **1989,** 111, 6183-6195.

54. H. Toftlund, *Coord. Chem. Rev.* **1989,** 94, 67-108.

55. H. Börzel, P. Comba, K.S. Hagen, Y.D. Lampeka, A. Lienke, G. Linti, M. Merz, H. Pritzkow, L.V. Tsymbal, *Inorg. Chim. Acta* **2002,** 337, 407-419.

56. H.-R. Chang, J.K. McCusker, H. Toftlund, S.R. Wilson, A. Trautwein, H. Winkler, D.N. Hendrickson, *J. Am. Chem. Soc.* **1990,** 112, 6814-6827.

57. T.J. Collins, *Acc. Chem. Res.* **1994,** 27, 279-385.

58. I.D. Cunningham, T.N. Danks, J.N. Hay, I. Hamerton, S. Gunathilagan, *Tetrahedron* **2001,** 57, 6847-6853.

59. I.D. Cunningham, T.N. Danks, J.N. Hay, I. Hamerton, S. Gunathilagan, C. Janczak, *J. Mol. Catal.* **2002,** 185, 25-31.

60. I.D. Cunningham, T.N. Danks, K.T.A. O'Connell, P.W. Scott, *J. Chem. Soc., Perkin Trans. 2* **1999**, 2133-2139.

61. A.C. Serra, E.C. Marçalo, A.M.d'A. Rocha Gonsalves, *J. Mol. Catal.* **2004,** 215, 17-21.

62. M. Ostermeier, C. Limberg, B. Ziemer, V. Karunakaran, *Angew. Chem. Int. Ed.* **2007,** 46, 5329-5331.

63. H. Kooijman, S. Tanase, E. Bouwman, J. Reedijk, A.L. Spek, *Acta Cryst.* **2006,** C62, m510-m512.

64. K.S. Hagen, *Inorg. Chem.* **2000,** 39, 5867-5869.

Figure Captions

Figure 1. Examples of non-heme iron(II) oxidation catalysts.

Figure 2. Backbone variations in bis(pyridylmethyl)diamine ligands **1** – **5**.

Figure 3. The molecular structure of [Fe(**2**)$(OTf)_2$].

Figure 4. Definition of the angle ϕ.

Figure 5. VT ^{19}F NMR spectra of complex [Fe(**2**)$(OTf)_2$] in CD_2Cl_2 between 198-298 K.

Figure 6. VT ^{19}F NMR spectra of complex [Fe(**3**)$(OTf)_2$] in CD_2Cl_2 between 198-298 K.

Figure 7. The magnetic moments of selected iron(II) complexes in CD_3CN solution as a function of temperature.

Figure 8. UV-vis spectra of iron bistriflate complexes of ligands **1** – **5** in CH_3CN (c = 0.5 mM).

Figure 9. Product distribution as a function of the equivalents of hydrogen peroxide added. Conditions: catalyst: 2.1 μmol [Fe(**1**)OTf_2], 2.1 mmol cyclohexane (1000 equiv.), room temperature in acetonitrile. The dashed line represents the total number of equivalents of oxidised product that can be obtained.

Figure 10. Product composition at various amounts of H_2O_2 in the oxidation of cyclohexane catalyzed by a) [Fe(**1**)$(OTf)_2$] and b) [Fe(**2**)$(OTf)_2$]. The dashed line represents the total number of equivalents of oxidised product that can be obtained.

Figure 11. Conversion of H_2O_2 into oxygenated products (A+2K curves) for different catalysts. The dashed line represents the total number of equivalents of oxidised product that can be obtained.

Graphical Abstract

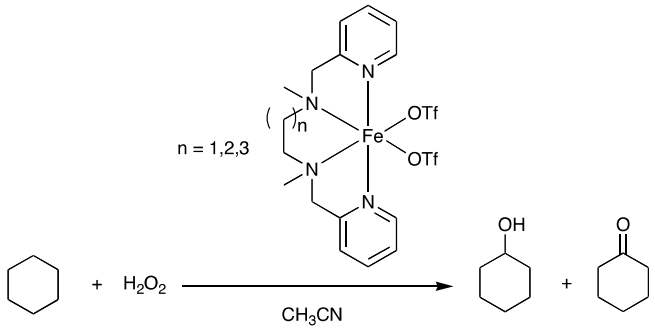

The catalytic activity of non-heme iron catalysts for the oxidation of alkanes with hydrogen peroxide is governed by the stability of the catalysts in the oxidising environment.